J. Fluid Mech. (2010), *vol.* 657, *pp.* 64–88.
doi:10.1017/S0022112010001369

Self-propulsion and dispersion of reactive colloids due to entropic anisotropy

HSIEN-HUNG WEI† AND JENG-SHIUNG JAN

Department of Chemical Engineering, National Cheng Kung University, Tainan 701, Taiwan

(Received 30 April 2009; revised 9 February 2010; accepted 14 March 2010;
first published online 17 June 2010)

In this paper, self-motion of reactive colloids and their dispersion behaviour are theoretically examined. The motion is driven by an osmotic force imbalance arising from non-uniform atmospheres of reactive solutes around the colloids. The propulsion here is not limited to Janus-like particles. It can also occur to particles having 'uniform' reactivity due to the more universal mechanism – entropic anisotropy created by breaking in rotational symmetry. The idea is demonstrated by examining the motion of a reactive particle due to asymmetry in its shape or to the presence of an additional particle. In the two-particle problem, in particular, we find that sink (source) particles can self-migrate towards (apart from) each other at velocities varying as R^{-2}, resembling Coulomb attraction (repulsion), where R is the inter-particle distance. Because of this Coulomb-like nature, a suspension of sink particles could undergo collective flocculation due to unscreened osmotic attraction. The criterion for an occurrence of the flocculation is also established. It reveals that the flocculation can occur if the particle volume fraction is within a certain window in terms of the solute concentration and the particle reactivity. The stability of reactive suspensions is also discussed using the modified Derjaguin–Landau–Verwey–Overbeek (DLVO) theory that takes account of the competition between long-range reaction-induced osmotic forces and short-range colloidal forces. A more generalized view for the present self-driven particle motion is elucidated by a simple scaling theory, providing lucid accounts for the self-motion of two particles, composite bodies, and Janus particles – all are driven by dipolar distortions in potential energy. Comparison with phoretic self-swimmers is also discussed.

1. Introduction

Control of the motion of colloidal particles is essential to self-assembly, micropatterning, synthesis and functionalization of nanoparticles and stability of suspensions. A common strategy for manipulating particles is to tune various short-range colloidal forces – the usual recipe based on classical Derjaguin–Landau–Verwey–Overbeek (DLVO) theory (Verwey & Overbeek 1948). One can achieve an active control on colloids to expedite the manipulation with external forces, for example, through electric/magnetic fields (Jones 1995; Morgan & Green 2003) and optical tweezers (Ashkin *et al.* 1986). Particles can also be driven by chemical potential gradients in various forms (e.g. electric potential, concentration and temperature) to move up against or down to the gradients, depending on their properties. A large class

† Email address for correspondence: hhwei@mail.ncku.edu.tw

of colloidal transport processes, so-called 'phoretic' phenomena (Anderson 1989), such as electrophoresis, diffusiophoresis, thermophoresis, etc., belong to this category.

While these strategies are useful in realizing a diversity of manipulations of colloidal particles, most of the attention is restricted to non-reactive impermeable colloids. In many practical applications, however, mass exchanges often occur between dispersed colloids and the bulk fluid. In one occasion, particles (e.g. catalysts) can uptake solutes from the bulk fluid, while in another (e.g. microemulsion or vesicles) they can be dissolved back into the bulk. In these situations, particles permit selective passages for solute or solvent molecules across the particle surfaces, acting like mobile sources/sinks with constant release/capture of their surrounding substances from/into themselves. From this point of view, these particles can be said 'reactive' because they possess specific chemical/physical affinities to the surrounding substances. For such particles, in addition to the usual colloidal forces, there exists another route to affecting their motion. Because of reactions, changes in local solute concentrations can create non-uniform atmospheres around the particles, giving rise to asymmetric entropic landscapes and hence in turn propelling them without needs in acquiring external forces or imposition of macroscopic potential gradients. That is, there will be autonomous motion sustained by the particles' own fuels. Indeed, such motion has been observed in solutions of reactive colloids (Howse *et al.* 2007) or nanosized objects (Paxton *et al.* 2004). Because the propulsion here is essentially generated by self-induced entropic fields, one might think it somewhat similar to colloidal phenomena due to overlapping depletion layer or excluded volume effects (Askura & Oosawa 1954), as observed in binary colloids (Crocker *et al.* 1999) and colloid–polymer mixtures (Ogden & Lewis 1996). And yet, as we will demonstrate, unlike the usual short-range colloidal effects, the nature of this reaction-driven entropic effect appears long range and hence can influence the particle motion distantly.

In this paper, we would like to explore more about how reactive colloids are propelled by entropic forces generated from their own. Although this subject has been investigated theoretically by several authors (Golestanian, Liverpool & Ajdari 2005, 2007; Córdova-Figueroa & Brady 2008), the efforts were focused on the motion of a single spherical particle with non-uniform reactivity. In practice, however, a particle could have some eccentricity on its shape, or, quite frequently, be surrounded by other particles. As such spatial anisotropy can also occur to a particle of 'uniform' reactivity, the effect can also create a 'non-uniform' solute concentration around the particle and hence produce an osmotic force to set it in motion. The present study will focus on the motion of reactive colloids of this kind. The paper is organized as follows. In § 2, we begin by reviewing the concept of symmetry breaking necessary for self-propulsion. This concept is first illustrated by examining the motion of a nearly spherical reactive particle in § 3. In § 4 we study the motion of two interacting reactive colloids. In § 5 we put forth to discuss possible impacts on the dispersion behaviour of reactive suspensions. The stability of reactive suspensions will also be examined in the modified DLVO framework. In § 6 we develop a simple scaling theory to elucidate the natures of self-driven entropic swimmers. § 7 is discussion. The paper is concluded in § 8.

2. Self-propulsion of reactive particles due to breaking in spatial symmetry

In the context of low-Reynolds-number hydrodynamics as assumed in most of the colloidal motions, the reversibility of flow (Happel & Brenner 1983) stipulates that a spherical particle having uniform reactivity does not migrate at all if it is placed in

an 'isotropic' medium. This is because the particle velocity $\boldsymbol{U}$ is linear in driving force $\boldsymbol{F}$ and the latter must vanish due to the perfect spatial symmetry.

Motion can be rendered if the particle loses its rotational symmetry due to a certain disparity in surface pattern or geometry, so that it can perceive unequal forces around itself. In other words, a symmetry breaking is produced by a prescribed direction, say, $\boldsymbol{p}$, along which a non-zero $\boldsymbol{F}$ can be generated by the particle itself and hence $\boldsymbol{U}$. This idea has been demonstrated using Janus particles having a dipole-like distribution of surface reactivity, as seen in diffusiophoretic self-swimmers (Golestanian *et al.* 2005, 2007) and osmotic motors (Córdova-Figueroa & Brady 2008). In § 6, we will discuss in more detail about how breaking in spatial symmetry leads to self-movement of particles and argue that particles can only migrate along $\boldsymbol{p}$.

For a particle with 'uniform' chemical activity, however, the only way to drive the particle without external forcing is to introduce asymmetry in its shape, place an additional boundary, or add an extra object around it. In this way, an anisotropic force field can also be produced to propel the particle. Prior to illustrating the effects at work, we first provide general formulism below for the problem.

Consider a particle with uniform surface activity immersed in a solution of smaller reactive solutes with diffusivity D. Neglecting convection, the solute concentration C is described by the diffusion equation:

$$D\nabla^2 C = 0, \tag{2.1}$$

subject to uniform concentration C_∞ far from the particle and the first-order reaction on its surface:

$$D\boldsymbol{n}\cdot\nabla C = k_s C \tag{2.2}$$

with the unit normal $\boldsymbol{n}$ pointing into the fluid. Here, the rate constant k_s can be either >0 if the particle (sink) uptakes the solutes, or <0 if the solutes are released from the particle (source) and dissolved back to the bulk phase.

As in Córdova-Figueroa & Brady (2008), the particle is propelled by an entropic/osmotic force arising from non-uniform solute concentration due to reaction. Despite some debates on such entropic propulsion (see e.g. the comments by Fisher & Dhar 2009; Jülicher & Prost 2009, and the replies by Córdova-Figueroa & Brady 2009*a*, *b*), the propulsion can be understood as follows. From statistical mechanics viewpoint, this force is a thermodynamic force generated by spatial variations of the probability density of solutes (i.e. the gradient of the configurational entropic energy) (Batchelor 1976). As shown by Squires & Brady (2005) as well as by Córdova-Figueroa & Brady (2009*b*), the propulsion here entails solutes to be somewhat 'visible' (in size, mobility or chemical activity) in distinction to the surrounding solvent at the Smoluchowski level, so that any anisotropy of the microstructure (i.e. the probability density distribution of solutes) around the particle can be transformed into a macroscopic force exerted by the solution on the particle. Speaking in a simple term, the particle can perceive an 'excess' osmotic pressure created by the non-uniformity of solutes around the particle. This entropy-driven mechanism is actually the basis of the Stokes–Einstein equation for determining the diffusion coefficient of a suspended object – the result by balancing the osmotic force with the Stokes drag, as derived by Einstein (Einstein 1905) a century ago.

As the force generated by spatial variations in the osmotic pressure Π over the particle surface S_p is $\boldsymbol{F}^{osm} = \int_{S_p} (-\Pi)\,\boldsymbol{n}\,\mathrm{d}A$ together with van Hoff's equation $\Pi = kTC$ (wherein kT is the thermal energy) by assuming that the solution is ideal (dilute), the

driving osmotic force can be written as

$$\boldsymbol{F}^{osm} = -kT \int_{S_p} C\boldsymbol{n}\,\mathrm{d}A, \tag{2.3}$$

which pushes the particle towards lower concentration regions. The particle velocity $\boldsymbol{U}$ is determined by $\boldsymbol{F}^{osm} + \boldsymbol{F}^{hyd} = 0$, zero total force through balancing $\boldsymbol{F}^{osm}$ with the hydrodynamic drag on the particle $\boldsymbol{F}^{hyd} = -\varsigma\boldsymbol{U}$. This yields

$$\boldsymbol{U} = \varsigma^{-1}\boldsymbol{F}^{osm} = -(kT/\varsigma)\int_{S_p} C\boldsymbol{n}\,\mathrm{d}A, \tag{2.4}$$

where ς is the drag coefficient. For a spherical particle, it can be seen immediately from (2.3) or (2.4) that to have a non-zero $\boldsymbol{F}^{osm}$ and $\boldsymbol{U}$, C must be even in $\boldsymbol{n}$. It thus follows that one needs at least a dipolar distortion in C (i.e. $C - C_\infty \propto \boldsymbol{x}/r^3$) for realizing the propulsion. Thereby, if the particle does not possess any inhomogeneity in its reactivity, its motion can only be realized by introducing some asymmetry to its shape or by the presence of other particles/boundaries, which will be examined next.

3. Self-migration of a nearly spherical reactive particle

We first examine the motion of a nearly spherical reactive particle. The particle has a mean radius of a with a small deformation over its periphery: $r = R(\theta) = a(1 + \varepsilon f(\theta, \phi))$, where $\varepsilon\,(\ll 1)$ is the amplitude of the deformation and $f(\theta, \phi)$ is the prescribed shape varying with both latitude θ and longitude ϕ. To solve C asymptotically, we expand it in ε : $C = C_0 + \varepsilon C_1 + \ldots$, with C_j satisfying (2.1) at every order j. Rewriting (2.2) as

$$D\left(\frac{\partial C}{\partial r} - \frac{1}{R^2}\frac{\partial R}{\partial \theta}\frac{\partial C}{\partial \theta} - \frac{1}{R^2\sin\theta}\frac{\partial R}{\partial \phi}\frac{\partial C}{\partial \phi}\right)N^{-1/2} = k_s C$$

with $N = 1 + R^{-2}(\partial R/\partial\theta)^2 + (R\sin\theta)^{-2}(\partial R/\partial\phi)^2$ and expanding it about $r = a$, we collect the terms in subsequent orders and solve the problem up to $O(\varepsilon)$ below.

At leading order, the problem satisfies $D\partial C_0/\partial r = k_s C_0$ at $r = a$ and $C_0 \to C_\infty$ as $r \to \infty$, and has a solution:

$$\frac{C_0}{C_\infty} = 1 - \left(\frac{\alpha}{1+\alpha}\right)\left(\frac{a}{r}\right). \tag{3.1}$$

Here $\alpha = k_s a/D$ is the ratio of the reaction rate to the diffusion rate. It is either >0 for sink particles or <0 for source particles (but we restrict $\alpha > -1$ to ensure $C_0(r = a) = 1/(1+\alpha) > 0$). In the reaction limit $|\alpha| \to 0$, $C_0/C_\infty \approx 1 - \alpha(a/r)$, whereas in the diffusion limit $\alpha \to \infty$ (which is only applicable to sink particles) has $C_0/C_\infty \approx 1 - (a/r)$, independent of α. At this order, it is obvious that the particle will not move at all since the concentration distribution here varies only radially – it is perfectly symmetric around the particle.

At next order $O(\varepsilon)$, we expect that the deformation will distort the concentration asymmetrically, which can be readily seen from the perturbed surface boundary condition:

$$\left(a^2 f(\theta,\phi)\frac{\partial^2 C_0}{\partial r^2} + a\frac{\partial C_1}{\partial r}\right) = \alpha\left(af(\theta,\phi)\frac{\partial C_0}{\partial r} + C_1\right) \text{ at } r = a. \tag{3.2}$$

Because $C_1 \to 0$ as $r \to \infty$, the solution can be expressed in a harmonic expansion:

$$\frac{C_1}{C_\infty} = \sum_m (a/r)^{m+1} A_m \,[\cdot]\, S_m, \tag{3.3}$$

where $[\cdot]$ denotes m scalar products between the mth-order polyadics A_m and S_m. The surface harmonics S_m are given by

$$S_m = (-1)^m r^{m+1} (\nabla \cdots \nabla)^m (1/r) \text{ or}$$

$$S_0 = 1, \quad \boldsymbol{S}_1 = \boldsymbol{n}, \boldsymbol{S}_2 = 3\boldsymbol{nn} - \boldsymbol{I}, \quad \text{etc.} \tag{3.4}$$

These surface harmonics satisfy the following orthogonal property over the surface (Anderson 1985):

$$\langle S_m S_\ell \rangle = \frac{1}{4\pi} \int\int S_m S_\ell \sin\theta \, \mathrm{d}\theta \, \mathrm{d}\phi = 0 \quad \text{if } m \neq \ell \tag{3.5}$$

with the first few orders listed below

$$\langle S_0 S_0 \rangle = 1, \quad \langle S_1 S_1 \rangle_{ij} = \tfrac{1}{3}\delta_{ij}, \quad \langle S_2 S_2 \rangle_{ijk\ell} = \tfrac{1}{3}(-2\delta_{ij}\delta_{k\ell} + 3\delta_{ik}\delta_{j\ell} + 3\delta_{i\ell}\delta_{jk}),$$

where δ_{ij} is the Kronecker delta. The coefficients A_m in (3.3) can be determined by substituting (3.3) into (3.2) and applying the orthogonal property (3.5). Expressing the deformation as a multipole expansion up to the quadrupole term: $f = f_0 + \boldsymbol{n}\cdot\boldsymbol{f}_1 + (3\boldsymbol{nn} - \boldsymbol{I})/2 : \boldsymbol{f}_2$, we find

$$A_0 = -\beta f_0 (2+\alpha)/(1+\alpha), \quad \boldsymbol{A}_1 = -\beta \boldsymbol{f}_1, \quad \boldsymbol{A}_2 = -(\beta/2)\boldsymbol{f}_2(2+\alpha)/(3+\alpha), \tag{3.6}$$

where $\beta = \alpha/(1+\alpha)$. Substituting (3.6) into (3.3) and evaluating $\boldsymbol{F}^{osm}$ in (2.4) (with $\varsigma \approx 6\pi\eta a$ and η the viscosity of the fluid), we find the particle velocity as

$$\boldsymbol{U} = \frac{2}{9}\frac{kTC_\infty a}{\eta}\frac{\varepsilon\alpha}{(1+\alpha)}\boldsymbol{f}_1. \tag{3.7}$$

Note here that the quadrupole deformation does not contribute to the velocity since the deformation is symmetric with respect to the midplane ($\theta = \pm\pi/2$). Hence, the particle will migrate in the direction along its principle axis $\boldsymbol{f}_1$. For a 'sink' particle ($\alpha > 0$), it will see a denser solute cloud on the blunt side than the sharp end (cf. A_1 in (3.6)), which in turn creates an osmotic pressure gradient pushing the particle towards the sharp end, as illustrated in figure 1(*a*). This result can be explained as follows. Near the sharp end where the local radius of the curvature is smaller, the diffusive flux from the bulk towards the particle surface is larger. As the solutes around the sharp end are consumed at faster rates than those on the blunt side, a net osmotic force will be created towards the sharp end where the solute concentration is lower, driving the particle to move in the same direction. Similarly, the motion of a 'source' particle ($-1 < \alpha < 0$) will be led by its blunt side, as illustrated in figure 1(*b*). An alternative but simpler explanation for the above motion behaviours is that one can view this slightly eccentric sphere as a composite object made by two touched spheres of different sizes – the larger one forms the blunt side and the smaller one does the sharp end (see § 5.2). Because the two sink (source) particles undergo inward (outward) osmotic forces and the larger one experiences a stronger force (see § 4 for the two-particle problem), the net force on the whole will be pointing towards the smaller (larger) one to drive the composite body towards that direction.

As indicated by (3.7) or shown in figure 2, the speed U of a sink particle can vary with α in different manners, depending on whether the swimming is reaction or

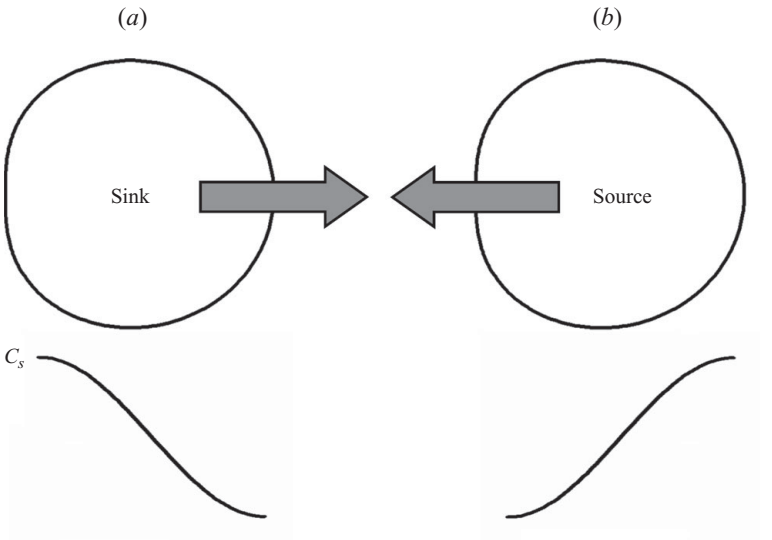

FIGURE 1. Schematic pictures for the self-swimming of a reactive sphere with a small dipolar deformation. (*a*) If the particle is sink-like ($\alpha > 0$), it will move in the direction towards its sharp end where the solute concentration is lower. (*b*) If the particle is source-like ($\alpha < 0$), the motion is just opposite to (*a*). The curves depict the solute concentration along the particle surface.

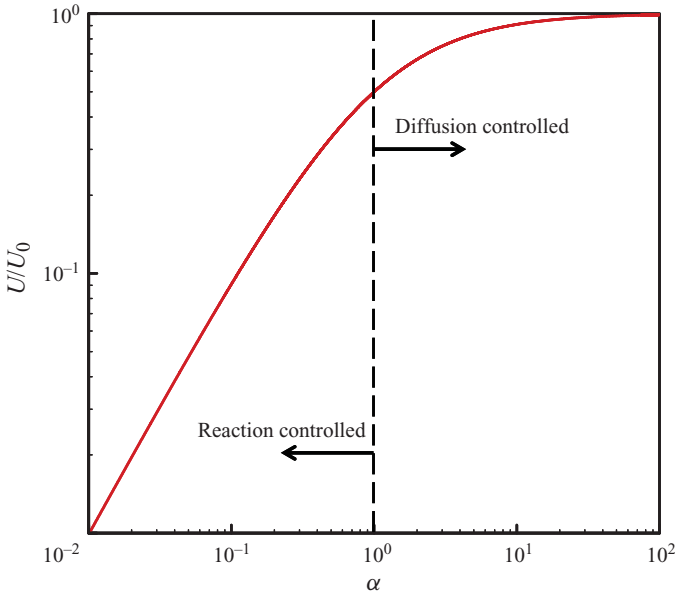

FIGURE 2. (Colour online) Drift velocity of a slightly deformed reactive sphere as a function of reactivity parameter α. The velocity here is normalized by $U_0 = (2/9)(kTC_\infty a\varepsilon/\eta)$.

diffusion controlled. If the reaction is slow $\alpha \ll 1$, $U \approx (2/9)\ (kTC_\infty \varepsilon a/\eta)\alpha \propto a^2$. If the reaction is fast $\alpha \gg 1$, however, the particle will no longer be speeded up by increasing α. In this limit, the particle reaches a maximum speed $U \approx (2/9)(kTC_\infty\, \varepsilon a/\eta) \propto a$. As for a source particle, its motion, because of the restriction $-1 < \alpha < 0$, will be limited

only by the reaction, since the reactants cannot be replenished indefinitely by the particle.

Different velocity scales shown above for sink particles can be obtained by simple scaling arguments below. For $\alpha \ll 1$, the particle is nearly impenetrable at slow reaction rates. As the concentration is now nearly uniform as in the bulk, it furnishes a reactive flux into the particle at the rate of $\sim k_s C_\infty$, giving rise to a concentration correction $C' \sim \varepsilon\, C_\infty k_s a/D \sim \varepsilon\, C_\infty \alpha$ through diffusion. The resulting osmotic pressure is then $\prod' \sim kTC' \sim kT\varepsilon\, C_\infty \alpha$. Balancing the osmotic force $\prod' a^2$ with the viscous drag $\eta U a$, the particle velocity is therefore $U \sim \prod' a/\eta \sim kT\varepsilon\, C_\infty a\, \alpha/\eta$. As for $\alpha \gg 1$, the reaction is so fast that the reactants are almost empty on the particle surface, except within the thin diffuse boundary layer of thickness $\delta_D \sim D/k_s$. The diffusion flux across the boundary layer now becomes $j_D \sim DC_\infty/\delta_D \sim k_s C_\infty$ and acts inwards towards the particle surface. It causes a concentration correction $C' \sim \varepsilon j_D/k_s \sim \varepsilon\, C_\infty$ through balance with the reaction, and thereby drives the particle at speed of $U \sim a\, kT\, C'/\eta \sim kT\varepsilon\, C_\infty a/\eta$.

4. Motion of two interacting reactive colloids

In the previous section, we have demonstrated that a slightly deformed reactive colloid can self-migrate, confirming the idea that it is necessary to have some prescribed direction to break spatial symmetry for rendering the propulsion. In this section, we will further elaborate this idea by considering a pair of reactive spheres in which the asymmetry is now created in the direction along their centre-to-centre line.

Two particles, labelled by 1 and 2, can be different in their sizes and reaction rates. Define the dimensionless reactivity $\alpha_i = k_{si} a_i/D$ for sphere i, where a_i and k_{si} denote the radius and reaction rate, respectively. If their centre-to-centre distance R is much larger than the particle sizes, the solute concentration satisfying (2.1) can be written as a twin harmonic expansion, stopping at the dipole terms by neglecting contributions from $O((a_1/R)^3, (a_2/R)^3)$ or higher:

$$\frac{C}{C_\infty} = 1 - \beta_1 \left(\frac{a_1}{r_1}\right) - \beta_2 \left(\frac{a_2}{r_2}\right) + A_1 \left(\frac{a_1}{r_1}\right)^2 \cos\theta_1 + A_2 \left(\frac{a_2}{r_2}\right)^2 \cos\theta_2 + \cdots \tag{4.1}$$

with $\beta_i = \alpha_i/(1+\alpha_i)$ $(i = 1, 2)$. Here we invoke two spherical coordinates (r_1, θ_1) and (r_2, θ_2) whose origins are located at the centres of sphere 1 and 2, respectively. Making use of Hobson's addition theorem (Hobson 1965):

$$\frac{1}{r_2} = \frac{1}{R}\left\{1 + \left(\frac{r_1}{R}\right)\cos\theta_1 + \cdots\right\}, \left(\frac{1}{r_2}\right)^2 \cos\theta_2 = \left(\frac{1}{R}\right)^2 \left\{1 + 2\left(\frac{r_1}{R}\right)\cos\theta_1 + \cdots\right\}, \quad \text{for } r_1 < R,$$

we can rewrite (4.1) in a single coordinate (r_1, θ_1) for $r_1 < R$:

$$\frac{C}{C_\infty} = 1 - \beta_1 \left(\frac{a_1}{r_1}\right) - \beta_2 \left(\frac{a_2}{R}\right)\left\{1 + \left(\frac{r_1}{R}\right)\cos\theta_1\right\} + A_1 \left(\frac{a_1}{r_1}\right)^2 \cos\theta_1 + A_2 \left(\frac{a_2}{R}\right)^2 + \cdots. \tag{4.2}$$

Applying boundary condition (2.2) at $r_1 = a_1$ on sphere 1, we can determine A_1 from the $\cos\theta_1$ term:

$$A_1 = \beta_2 \left(\frac{a_1 a_2}{R^2}\right)\left(\frac{\alpha_1 - 1}{\alpha_1 + 2}\right). \tag{4.3}$$

Equation (4.3) bears the similar form to the Clausius–Mossotti factor in polarization induced by electric fields (Pohl 1978), and agrees with the dipole coefficient of the exact solution obtained previously (Tsao 2001). Similarly, A_2 can be determined by evaluating (2.2) on the surface of sphere 2, or simply obtained by interchanging subscripts 1 and 2 in the expression of A_1. Substituting (4.3) into (4.2) and writing $\cos\theta_1 = \boldsymbol{n}_1 \cdot \boldsymbol{e}_R$ as the projection of the surface normal $\boldsymbol{n}_1$ on the centreline direction $\boldsymbol{e}_R$ (pointing towards sphere 2), we find the solute concentration distribution around sphere 1:

$$\frac{C(r_1 = a_1)}{C_\infty} \approx 1 - \beta_1 - \beta_2 \left(\frac{a_2}{R}\right) + A_2 \left(\frac{a_2}{R}\right)^2 - \left(\frac{3\beta_2}{2+\alpha_1}\right)\left(\frac{a_1 a_2}{R^2}\right) \boldsymbol{n}_1 \cdot \boldsymbol{e}_R. \tag{4.4}$$

Here, we are only interested in the last term, since this term varies with azimuthal position and is able to reflect the non-uniformity in the solute concentration between the particles. As a result, sphere 1 has lower (higher) solute concentration on its front hemisphere $-\pi/2 < \theta_1 < \pi/2$ due to the uptake (release) of the solutes by sphere 2 with $\beta_2 > 0\,(< 0)$. That is, the solute distribution now becomes anisotropic because they are re-distributed around the dumbbell-like geometry. Evaluating (2.4) with the osmotic force on sphere 1: $\boldsymbol{F}_1^{osm} = -kT \int C(r_1 = a_1)\boldsymbol{n}_1 \mathrm{d}A$, we find the velocity of sphere 1 as

$$\boldsymbol{U}_1 \approx \frac{2kTC_\infty a_2}{3\eta} \frac{\alpha_2}{(1+\alpha_2)(2+\alpha_1)} \left(\frac{a_1}{R}\right)^2 \boldsymbol{e}_R. \tag{4.5a}$$

Similarly, for sphere 2 we have

$$\boldsymbol{U}_2 \approx -\frac{2kTC_\infty a_1}{3\eta} \frac{\alpha_1}{(1+\alpha_1)(2+\alpha_2)} \left(\frac{a_2}{R}\right)^2 \boldsymbol{e}_R. \tag{4.5b}$$

Here we neglect hydrodynamic interactions between the particles because the associated corrections to the particle velocities are of $O(U_1 a_1/R, U_2 a_2/R)$ or smaller. Equations (4.5*a*, *b*) indicate that the particles will migrate along their centreline. Since the direction of $\boldsymbol{U}_i$ of one particle is determined by the sign of the reactivity α_j of the other, the particles can either move towards or depart from each other, depending on if $\alpha_j > 0$ or < 0, as will be discussed in more details in § 4.2.

4.1. *Swimming at low and high reaction rates*

As indicated by (4.5), at low reaction rates the velocity of one particle $U_1 \sim (kTC_\infty a_2/\eta)\alpha_2 (a_1/R)^2$ is controlled by the reaction of the other (via α_2). This also suggests that a non-reactive particle ($\alpha_1 = 0$) can be propelled by a stationary sink (source) and move towards (away from) it. For a pair of 'sink' particles at high reaction rates, however, the motion of one particle is limited by the particle's own reaction and inversely proportional to its reaction rate, viz., $U_1 \sim (kTC_\infty a_2/\eta)(1/\alpha_1)(a_1/R)^2$. As a particle is in effect self-propelled by the concentration distortion due to the influence of its nearby partner, the above results can also be explained by simple reflection mechanisms below.

At low reaction rates, one reactive particle, say, sphere 2, creates a solute cloud of $C_\infty \alpha_2 (a_2/r_2)$ around itself. Because this cloud is perturbed by the presence of sphere 1 at $r_2 = R$, sphere 1 will perceive a small concentration change $C' \sim C_\infty \alpha_2 (a_2/R)(a_1/R)$ from sphere 2, producing an osmotic force on sphere 1 and hence driving sphere 1 at velocity $U_1 \sim a_1 kT\, C'/\eta \sim (kTC_\infty a_2/\eta)\alpha_2 (a_1/R)^2$. At high reaction rates (only applicable to sink particles here), the concentration around sphere 2 is $C_\infty (a_2/r_2)$ with $C' \sim C_\infty (a_2/R)(a_1/R)$ due to the presence of sphere 1. Since the solute transport is now controlled by diffusion, the concentration on the surface of sphere 1 due to C' is

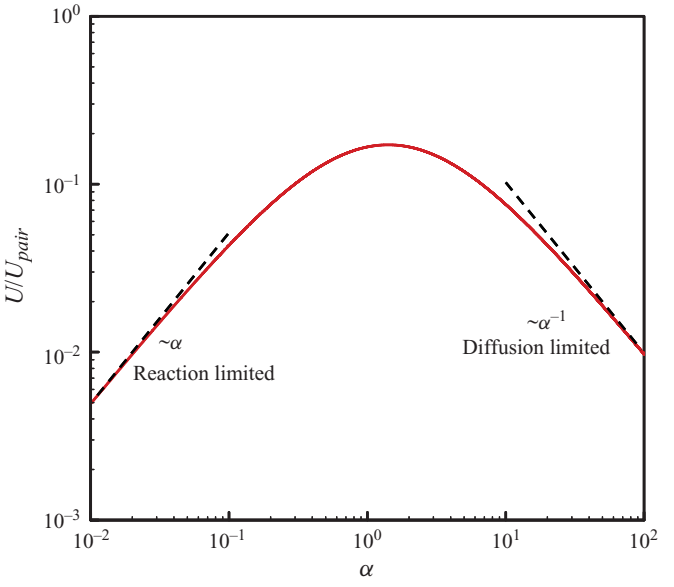

FIGURE 3. (Colour online) Effects of reactive parameter α on drift velocity U of a sink particle due to osmotic attraction by its twin partner. Because U grows linearly with α for small α but decays like α^{-1} for large α, it must exist a maximum in the range of α. The velocity here is scaled by $U_{pair} = (2/3)(kTC_\infty a/\eta)(a/R)^2$.

$C_s' \sim j_D/k_{s1}$ sustained by the diffusion flux $j_D \sim DC'/a_1$. The effect therefore propels the particle at velocity $U_1 \sim a_1 kT\, C_s'/\eta \sim (kTC_\infty a_2/\eta)\,(1/\alpha_1)(a_1/R)^2$.

In the special case where two sink particles are identical, the particle speed at low reaction rates (small α) is $U = (1/3)(kTC_\infty a/\eta)\alpha(a/R)^2 \propto k_s a^4$ which can be increased by raising the reaction rate. At high reaction rates (large α), on the other hand, $U = (2/3)(kTC_\infty a/\eta)(1/\alpha)(a/R)^2 \propto k_s^{-1}a^2$ decreases with the reaction rate. These two limiting scenarios suggest that there must exist a maximum velocity in the range of α, as shown in figure 3. This maximum thrust occurs at a moderate $\alpha(=2^{1/2})$ when the reaction rate is comparable to the diffusion rate, which can be explained as follows. While the particles can be propelled with more fuels by increasing the reaction rate, reactants around the particles could be insufficient to sustain the motion. That is, the particles could be slowed down by over-consumption of reactants. Thereby, the maximum thrust can only be realized by reconciling consumption and replenishment of reactants in the range of moderate reaction rates.

At a constant reaction rate k_s, small (large) α means small (large) particles in use. Since $U \propto a^4$ at small α and $U \propto a^2$ at large α, it is possible to use particles in different sizes in experiments to see which scale the velocity follows and hence to distinguish whether the drift is controlled by reaction or by diffusion.

4.2. *Coulomb-like attraction/repulsion due to inter-particle entropic landscapes*

As indicated by (4.5), two sink particles ($\alpha > 0$) will migrate towards each other, whereas a source pair ($\alpha < 0$) will move apart. This pairwise motion looks as if the particles were attracted towards or repelled from each other, resembling the motion due to electrostatic interactions. Such Coulomb-like motion is further signified by the $1/R^2$ attenuation in the particle velocities. As illustrated in figure 4, such motion can be thought of being driven by an entropic landscape in between the particles. For two

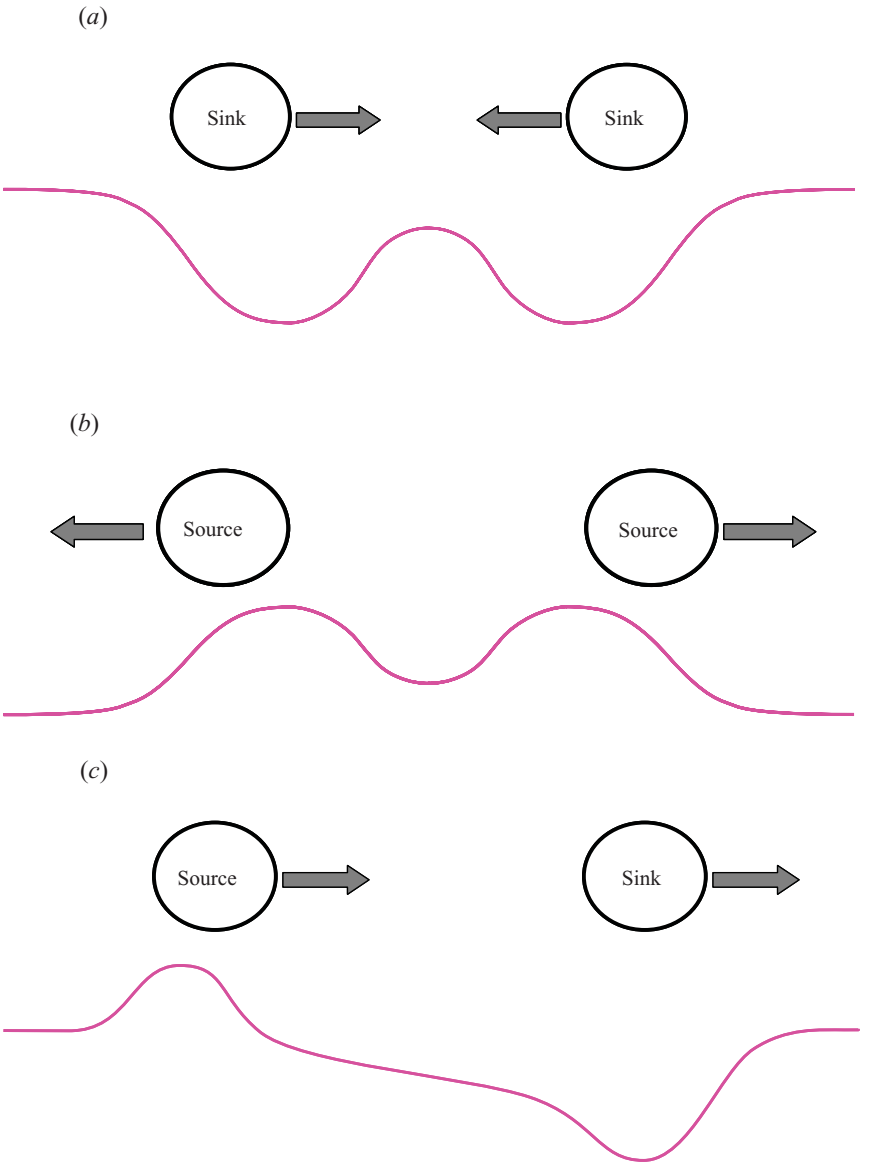

FIGURE 4. (Colour online) Schematic pictures of the motion of two reactive particles. (*a*) A pair of sink particles can be attracted towards each other, since the particles experience relatively lower solute solutions on the interior side of the pair. As illustrated by the profile of the solute concentration, the situation here is somewhat similar to that of two heavy balls placed on a soft sheet: one ball can bend the sheet and create a basin around it; placing another nearby will lead the two to fall onto each other because of deeper sinking of the basin. (*b*) Similarly, a pair of source particles will be repelled from each other. (*c*) For an unlike pair, both source and sink particles will move in the same direction led by the sink. The curves depict the corresponding profiles of the solute concentrations.

interacting sink particles, they tend to suck solute molecules around them. Because the solute concentrations far from the particles must remain higher than those nearby, an entropic 'bulge' must exist in between the particles (figure 4*a*). As more solutes can be consumed in the region between the particles, the height of this bulge is lower

than the bulk level. As a result, the solute concentration around one particle on the side in the inter-particle region is lower, creating a lower osmotic pressure to draw the particle towards its partner. The situation here looks more like two heavy balls placed on a soft sheet – one ball can bend the sheet and create a basin around it; placing another ball nearby will lead all to fall onto each other because of deeper sinking of the basin. Similarly, two source particles will be separated by an elevated energy hill in between, causing them to move apart (figure 4*b*).

Similar to the method of image charge in electrostatics, an identical reactive pair in an unbounded fluid can be thought of as twin images with respect to their midplane, so their motion is equivalent to that of a particle having a large distance above an impenetrable or reaction-inert plane (provided that hydrodynamic interactions are negligible). Thus, the motion of twin particles (with $a_1 = a_2 = a$ and $k_{s1} = k_{s2}$) implies that a sink (source) particle can also self-migrate towards (away from) the plane. In this case, the particle velocity is still given by (4.5) but with R replaced by $2d$, twice the distance from the particle to the plane.

Now consider the motion of an unlike pair. As the source (sink) particle tends to move towards (away from) its partner, they all drift in the same direction led by the sink particle (figure 4*c*). In this case, whether they can run into together depends on if the source particle (sphere 1 with $-1 < \alpha_1 < 0$) is fast enough to catch up with the sink particle (sphere 2 with $\alpha_2 > 0$). Inspecting the velocity ratio of these two particles, we find

$$\frac{|\boldsymbol{U}_1|}{|\boldsymbol{U}_2|} = \frac{k_{s2}}{|k_{s1}|}\left(1 - \frac{1}{2 - |\alpha_1|}\right)\left(1 + \frac{1}{1 + \alpha_2}\right) \leqslant \frac{k_{s2}}{|k_{s1}|}. \tag{4.6}$$

As this velocity ratio never exceeds inverse the corresponding reaction-rate ratio, the source will never catch up with the sink if the rate of reactants consumed by the sink is lower than that produced by the source. It is also evident that the faster consumption rate the sink particle has, the more likely for it to be captured by the source particle.

Finally, we should emphasize that the particle velocity here attenuates at the rate of $1/R^2$, which is slower than $1/R^3$ in phoretic interaction. In fact, as will be shown in §§ 6 and 7.3, such a Coulomb-like drift is a generic feature of entropic swimmers. As the corresponding potential energy decays like $1/R$ and acts like an unscreened electrostatic potential, this character imparts 'long-range' influence on the dispersion behaviour of reactive colloids, possibly destabilizing dilute suspensions (by attraction) or stabilizing concentrated suspensions (by repulsion). This also leads to our conjecture that sink colloids could undergo collective flocculation, which will also be discussed later in § 5.1.

4.3. *Near-contact motion of two sink particles*

For two interacting sink particles with a large separation $h(= R - 2a \gg a)$, we have learned from (4.5) that they will move towards each other at the speed increasing at the rate of h^{-2} because of steepening in solute concentration gradients. However, the particles cannot be speeded up indefinitely. This is because when their separation is decreased, the particles will also experience gradually increasing hydrodynamic drags, making them slowed down during this mutual attraction process. This implies that the particle velocity will not vary monotonically with h – a maximum velocity must exist at a certain particle separation.

To see how the particles are slowed down by their mutual approaching, we consider the opposite extreme in which the two particles come so close that their separation becomes much smaller than the particle size ($h \ll a$). Here we do not intend to

solve the problem in detail, though it can be rigorously formulated using matched asymptotic expansions (Solomentstev, Velegol & Anderson 1997). Instead, we employ a simple scaling analysis below to elicit the physics for such a near-contact situation.

In the thin gap region, the solute transport is dictated by diffusion across the gap: $\partial^2 C/\partial z^2 \approx 0$, where z measures the normal distance to the midplane. As the diffusion rate $D\partial C/\partial z \sim DC/h$ is also much faster than the reaction rate $k_s C$ (provided that $\alpha = k_s a/D$ is $O(1)$), the particles look virtually impenetrable, viz., $\partial C/\partial z \approx 0$, which admits a uniform concentration, say, C_0, across the gap. Outside the gap, however, solutes can now be consumed by the reaction. This causes the concentration outside the gap to be lower than that in the gap and hence the osmotic pressure. As a result, the lower osmotic pressure outside the gap will suck the fluid out, bringing the particles further closer as required by fluid mass conservation.

Having the above picture in mind, we estimate relevant scales below. As the solute transport here is essentially controlled by reaction, any non-uniformity of the solute concentration within the gap must arise from variations in axial diffusion. This axial diffusion creates a concentration $C' \sim \alpha C_0(h/a)$ deviated from C_0 and hence an osmotic pressure $\Pi' \sim \alpha kTC_0(h/a)$ for the propulsion. Since this pressure actually varies laterally over the length scale $\ell \sim (ha)^{1/2}$ and decreases towards the proximate bulk, its gradient drains the fluid with the lateral velocity $V \sim h^2\Pi'/\eta\,\ell$. Also because the fluid mass must be conserved, the particles will squeeze the fluid and head towards each other with $U \sim (h/\ell)V$. Given the fact that C_0 is nearly of an order of C_∞ (More precisely, it can be identified using matched asymptotic techniques that $C_0/C_\infty \sim (h/a)^{\sqrt{2}-1}$, similar to the analogous heat conduction problem considered by Solomentstev *et al.* 1997.), the particle velocity can be estimated by

$$U \sim \frac{akTC_\infty\alpha}{\eta}\left(\frac{h}{a}\right)^3. \tag{4.7}$$

Hence, in contrast to the h^{-2} velocity attenuation in the large-separation limit, the particle velocity in the small-gap limit grows with h^3. Hence, a maximum drift velocity U_{max} must exist in such a way that solute concentration gradients are steepened by deceasing h from the large-separation limit and viscous drags are decreased by increasing h from the thin-gap limit. That is, $U_{max} \sim akTC_\infty\alpha/\eta$ can be found at the crossover distance, $h^* \sim a$, between these two limits. In figure 5 we demonstrate such a transition by displaying how the particle velocity varies with the inter-particle distance in both small and large separation limits.

5. Dispersion of reactive colloids

5.1. *Flocculation of sink particles*

Recall in § 4.2 that two sink particles can migrate towards each other in a Coulomb-like manner. If such long-range attraction-like motion enables bringing these particles to a sufficiently short distance within which their natural short-range attraction forces are strong, they might eventually collide and even be bound to each other. In other words, a suspension of sink particles might be susceptible to flocculation. In this section, we will investigate this reaction-induced flocculation and find the conditions under which the flocculation can occur.

From a kinetic point of view, the flocculation can only occur if the inter-particle attraction is not significantly disrupted by Brownian randomization between these colloids. That is, the flocculation must occur sufficiently fast in such a way that

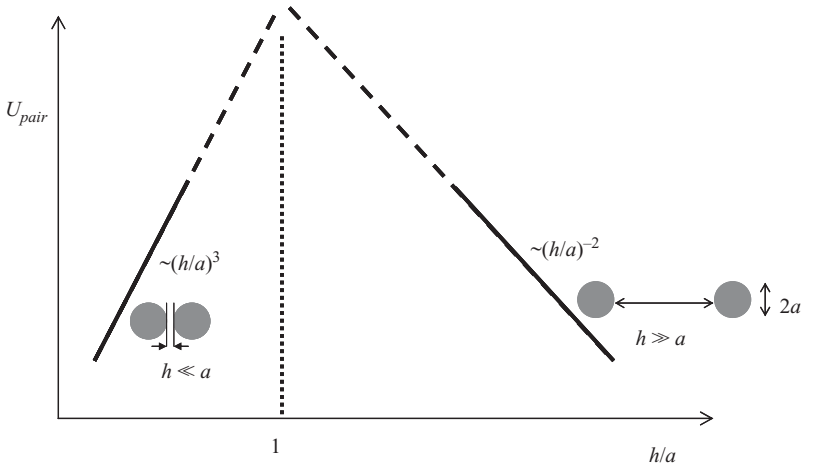

FIGURE 5. An illustration of how the pairwise velocity U_{pair} varies with the particle separation-to-size ratio h/a.

the particle collision time $\tau_U \sim R/U$ is shorter than the macroscopic diffusion time $\tau_R \sim R^2/D_{eff}$ over the particle separation R. Alternatively, Brownian displacements of the particles $\Delta\ell \sim (D_{eff}\tau_U)^{1/2}$ during τ_U must be no larger than R. Here D_{eff} is the effective particle diffusivity resulted from enhancement by reaction and is given by (Golestanian *et al.* 2007; Howse *et al.* 2007)

$$D_{eff} = D_p + U^2\tau_a/6, \tag{5.1}$$

where $D_p \sim kT/\eta a$ is the native particle diffusivity and $\tau_a \sim a^2/D_p$ is the rotational diffusion time over the particle size. As such, there are three time scales involved: the collision time τ_U, the macroscopic diffusion time τ_R and the microscopic diffusion time τ_a. The condition $\tau_R > \tau_U$ entails the macroscopic Peclet number, the ratio between these two time scales, to be larger than unity:

$$Pe_R = \frac{\tau_R}{\tau_U} = \frac{UR}{D_{eff}} > 1. \tag{5.2}$$

Because $\tau_R \sim R^2/D_{eff}$ and D_{eff} is determined by how fast the particle drift U is compared to the rotational diffusion speed $a/\tau_a \sim D_p/a$, we also have to invoke the microscopic Peclet number to measure the ratio between these two velocity scales:

$$Pe_a = \frac{Ua}{D_p}. \tag{5.3}$$

Below we will use (5.2) to establish the criterion for realizing the flocculation in both $Pe_a \ll 1$ and $Pe_a \gg 1$ limits.

For $Pe_a \ll 1$, the particles are Brownian-like with $D_{eff} \sim D_p$ from (5.1). Hence, (5.2) becomes

$$Pe_R = \frac{\tau_R}{\tau_U} = \frac{UR}{D_p} > 1 \text{ for } Pe_a \ll 1. \tag{5.4}$$

Making use of $D_p \sim kT/\eta a$ and $U \sim \gamma akTC_\infty(a/R)^2/\eta$ with $\gamma = \alpha/((1+\alpha)(2+\alpha))$ from (4.5), (5.4) can be rewritten as $\gamma a^3 C_\infty(a/R) > 1$, namely

$$\phi > (C_\infty a^3\gamma)^{-3}, \tag{5.5}$$

where $\phi \sim (a/R)^3$ is the volume fraction of the particles. Equation (5.5) is the condition for realizing the flocculation of Brownian reactive particles ($Pe_a \ll 1$). It provides the minimum particle fraction for an onset of the flocculation. It is also evident that the larger particle size and the higher reactant concentration, the more inclination to the flocculation.

At the other extreme $Pe_a \gg 1$, the particles' rotational diffusion is suppressed. Since the particle drift can now be enhanced by reaction, we have $D_{eff} \sim U^2\tau_a$ from (5.1). Equation (5.2) then becomes

$$Pe_R = \frac{UR}{D_{eff}} \sim \frac{R}{U\tau_a} \sim \frac{\tau_U}{\tau_a} > 1 \text{ for } Pe_a \gg 1. \tag{5.6}$$

This leads the collision time to be longer than the microscopic diffusion time. Substituting $\tau_U \sim R/U \sim \eta/\gamma kTC_\infty\phi$ and $\tau_a \sim \eta a^3/kT$ into (5.6), we find that flocculation can occur to non-Brownian reactive particles ($Pe_a \gg 1$) if the following condition is satisfied:

$$\phi < (C_\infty a^3\gamma)^{-1}. \tag{5.7}$$

At the particle concentration beyond the critical value above, although the particle drift can be promoted by increasing the particle fraction (because $U \sim \gamma akTC_\infty\phi^{2/3}/\eta$), it will be soon outweighed by its own drift-enhanced Brownian motion, thereby keeping the particles from aggregation.

Equations (5.4) and (5.6) suggest that for arbitrary Pe_a, the criterion for realizing flocculation of sink particles is that the characteristic collision time must be within the range between the macroscopic and microscopic particle diffusion times:

$$\tau_a < \tau_U < \tau_R, \tag{5.8}$$

wherein $\tau_a \sim \eta a^3/kT$, $\tau_U \sim \phi^{-1}\eta/\gamma kTC_\infty$ and $\tau_R \sim \phi^{-2/3}\eta a^3/kT$ for $Pe_a \ll 1$. This criterion therefore furnishes conditions (5.5) and (5.7) combined:

$$(C_\infty a^3\gamma)^{-3} < \phi < (C_\infty a^3\gamma)^{-1}, \tag{5.9}$$

providing the range of the particle volume fraction within which the flocculation can occur. Also, because (5.9) is only applicable to dilute suspensions $\phi \ll 1$, this requires

$$C_\infty a^3\gamma \gg 1. \tag{5.10}$$

Thereby, (5.10) suggests that for micrometre-sized particles, their flocculation requires the addition of reactive reagents at $C_\infty \gg 10^{-9}$M, which can be realized in most of the common systems.

The reasons for the existence of such a window of the particle volume fraction can be understood as follows. On the one hand, too concentrated particles can undergo intense reaction-enhanced Brownian randomization and hence inhibit clustering driven by mutual attraction between the particles. If the suspension is too dilute, however, the movement of the particles will be too sluggish to cause aggregation, since solute concentration gradients (and hence osmotic forces) between far apart particles are insufficient to drive the particles. Figure 6 is a map that summarizes how the time scales discussed above depend on the particle volume fraction. It depicts how the particle dispersion behaviour is determined by these time scales. The susceptibility to the flocculation discussed by far does not include short-range van der Waals and electrostatic interactions. How these effects mediate the stability of reactive suspensions will be discussed next.

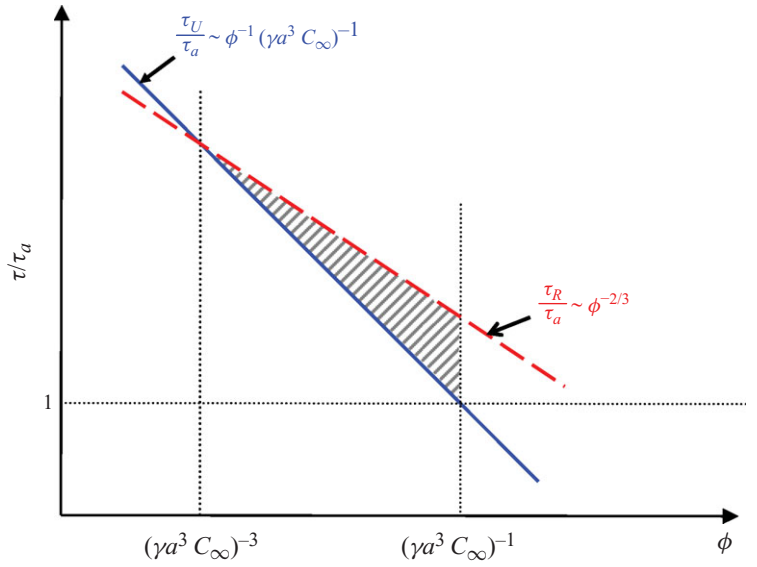

FIGURE 6. (Colour online) Time scales involved in affecting the dispersion of a suspension of sink colloids: the collision time τ_U, the macroscopic diffusion time τ_R, and the microscopic diffusion time τ_a. These time scales have different dependences on the particle volume fraction ϕ. Flocculation can occur when $\tau_a < \tau_U < \tau_R$ in the range of ϕ, as indicated by the shaded area.

5.2. *Stability of reactive suspensions*

As shown earlier, reactive colloids can be self-attracted or repelled in a Coulomb-like manner due to reaction-induced osmotic effects. An important implication from this long-range feature is that reactive colloids could become more agglomerative or more dispersive than inert ones. In the preceding subsection, we have shown that sink-like colloids could be inclined to flocculation due to this mechanism. And yet, since actual processes further involve short-range van der Waals and electrostatic forces that could encourage or discourage attraction/repulsion between particles, the ultimate fate of reactive colloids seems to rely on how long-range osmotic forces compete with these short-range colloidal forces. Hence, in this part of discussion, we modify the classical DLVO theory by including the osmotic effects to examine the stability of reactive suspensions.

For a pair of reactive colloids of size a and separation $R(>2a)$, the inter-particle potential Ψ consists of three parts: the van der Waals attraction potential $\Psi_{vdw}(<0)$ (Russel, Saville & Schowalter 1989), the pairwise Yukawa potential $\Psi_{el}(>0)$ accounting for the screened Coulomb repulsion (Verwey & Overbeek 1948) and the osmotic attraction/repulsion potential Ψ_{rxn} induced by reaction:

$$\Psi = \Psi_{vdw} + \Psi_{el} + \Psi_{rxn} = -\Psi^0_{vdw} H(R/a) + \Psi^0_{el} \exp(-\kappa R)\left(\frac{a}{R}\right) + \Psi^0_{rxn}\left(\frac{a}{R}\right). \quad (5.11)$$

In the van der Waals part, $\Psi^0_{vdw} = 16A_H/9$ with A_H being the Hamaker constant having magnitude in the thermal energy kT, and $H(R/a) = (3/32)[2(a/R)^2 + 2a^2/(R^2 - 4a^2) + \ln(1 - 4(a/R)^2)]$ (Russel *et al.* 1989). Since the contributions from the other two parts are merely accounted at sufficiently large R, for consistency we take $H(R/a) \approx (a/R)^6$ in the large-R form. In the electrostatic part, $\Psi^0_{el} = (q^2/\varepsilon_m a)\exp(2\kappa a)/(1+\kappa a)^2$ with q being the charge of the colloids, κ^{-1} the Debye

screening length and ε_m the dielectric constant of the solution. In the osmotic part, Ψ^0_{rxn} has $kTC_\infty a^3\gamma$ in magnitude and can be either >0 for repulsion between source particles, or <0 for attraction between sink particles.

If the colloids are source-like, they tend to keep apart from each other because $\Psi_{rxn} > 0$. Since this tendency will be enhanced by electrostatic repulsion but mitigated by van der Waals attraction, we only focus on the latter's effects on the stability of the system at high ionic strengths ($\kappa \to \infty$). Inspecting (5.11) in the $\kappa \to \infty$ limit, we find that Ψ admits a maximum $\Psi_{max} = 5(\chi/6)^{6/5}\Psi^0_{vdw}$ at $R_{max} = a(6/\chi)^{1/5}$, where $\chi \equiv \Psi^0_{rxn}/\Psi^0_{vdw}$ measures the relative magnitude of the osmotic repulsion with respect to van der Waals attraction. Therefore, the maximum can only exist if $R_{max}/a = (6/\chi)^{1/5} > 2$ or $\chi < \chi^* = 3/16$ under which $\Psi_{max}/\Psi^0_{vdw} < 5/64$. It follows that if $\Psi^0_{rxn} > \chi^*\Psi^0_{vdw} = A_H/3$, Ψ will decrease monotonically in R – van der Waals attraction is too weak to oppose the osmotic repulsion. Hence, the colloids will always remain separated. On the other hand, if $\Psi^0_{rxn} < \chi^*\Psi^0_{vdw}$, the colloids would have an opportunity to be gathered by their van der Waals attraction which is now strong enough to overcome the osmotic repulsion. In figure 7(*a*), we plot Ψ/Ψ^0_{vdw} as a function of R/a for various values of χ. The result shows that the repulsion is indeed suppressed by van der Waals attraction as χ is decreased, and the existence of energy maxima for $\chi < 0.2$, as described above. However, since the energy barrier Ψ_{max} for this dispersion–aggregation transition is $(5/64)\Psi^0_{vdw} = (5/36)A_H$ and is smaller than the thermal energy kT, we surmise that aggregation, if it occurred, would hardly be maintained due to thermal fluctuations.

As for sink particles, they tend to aggregate due to the osmotic attraction with $\Psi_{rxn} < 0$. As this tendency, with or without van der Waals attraction, can only be resisted by electrostatic repulsion, we set $\Psi^0_{vdw} = 0$ in (5.11) to see how the electrostatic repulsion alone competes with the osmotic attraction. It is clear that there is no way to stop the aggregation in the limit of $\kappa^{-1} \to 0$ at which Ψ_{el} vanishes completely because of the Debye screening. In the limit of $\kappa^{-1} \to \infty$, the aggregation can simply be prevented by electrostatic repulsion with $q^2/\varepsilon_m a > |\Psi^0_{rxn}|$. For finite κ^{-1}, an equilibrium can be established between the osmotic attraction and electrostatic repulsion, creating an energy well Ψ_{min} at $R = R_{min}$. Here R_{min} is determined by $\Lambda = g(R)$ from $\mathrm{d}\Psi/\mathrm{d}R = 0$, where $g(R) \equiv \exp(\kappa R)/(\kappa R + 1)$ and $\Lambda \equiv \Psi^0_{el}/|\Psi^0_{rxn}|$ measures the strength of electrostatic repulsion relative to the osmotic attraction. Since $g(R)$ increases monotonically in $R(>2a)$, an equilibrium (i.e. energy minimum) can only exist if $\Lambda > \Lambda^* = g(2a) = \exp(2\kappa a)/(2\kappa a + 1)$. That is, one requires $q^2/\varepsilon_{\mathrm{m}} a > |\Psi^0_{rxn}|(\kappa a + 1)^2/(2\kappa a + 1)$ to defeat the attraction for keeping the colloids from aggregation. Figure 7(*b*) portrays the distributions of $\Psi(R)$ for various values of Λ when $\kappa a = 0.8$. The result indicates that the osmotic attraction is diminished by electrostatic repulsion as Λ is increased, and that an energy minimum begins to emerge when $\Lambda > \Lambda^* \approx 2$, confirming the features described above.

6. Self-driven particle motion due to dipolar distortion in potential energy

In § 3, we have demonstrated the self-migration of a slightly eccentric reactive particle. We have also shown in § 4 that two reactive colloids can self-approach or move apart from each other. These self-driven motions, because of asymmetries in the geometries, are driven by osmotic forces arising from non-uniform solute concentrations around particles. In fact, this kind of locomotion is not limited by that powered by reaction. A similar motion can also be realized by other means such as temperature or electrical potential. In this section, we do not intend to make

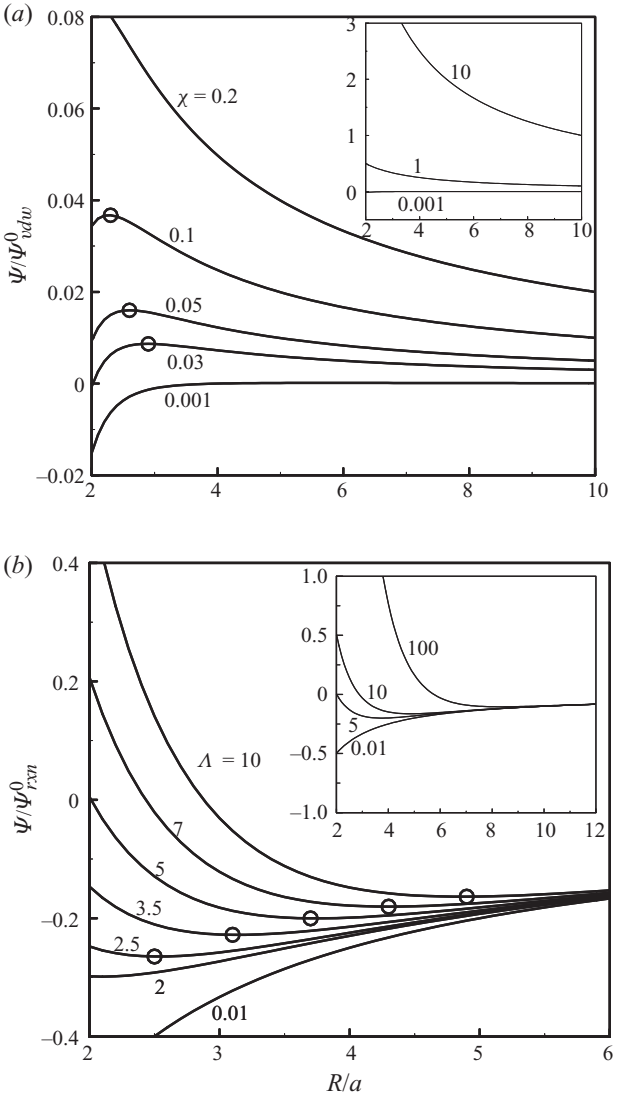

FIGURE 7. Pair potential energy landscapes for reactive colloids in the presence of van der Waals and electrostatic effects. (*a*) Effects of van der Waals attraction on potential distributions for source particles ($\Psi^0_{rxn} > 0$). The parameter $\chi = \Psi^0_{rxn}/\Psi^0_{vdw}$ measures the relative magnitude of the reaction-induced osmotic repulsion with respect to van der Waals attraction. The osmotic repulsion is suppressed by van der Waals attraction as χ is decreased. For $\chi < \chi^* \approx 0.2$, energy maxima start to appear, as indicated by circles. Inset is a larger scale view on how the potential energy behaves when χ varies from small to large values. (*b*) Effects of electrostatic repulsion (with $\kappa a = 0.8$) on potential distributions for sink particles ($\Psi^0_{rxn} < 0$). $\Lambda = \Psi^0_{el}/|\Psi^0_{rxn}|$ measures the strength of electrostatic repulsion relative to the reaction-induced osmotic attraction. The osmotic attraction is diminished by electrostatic repulsion as Λ is increased. For $\Lambda > \Lambda^* \approx 2$, energy minima (equilibria) can exist, as indicated by circles. Inset is a larger scale view on how the potential energy behaves when Λ varies from small to large values.

formal mathematical generalization. Instead, we develop a scaling theory to explain self-driven motion of various systems in a unified view. As will be seen below, this theory, though qualitative, provides a lucid way to reveal the essences of self-driven phenomena. As we will also show, the present autonomous particle motion is actually

a new class of self-driven phenomena that are driven by dipolar distortions in potential energy. We start with the motion of two interacting particles. We then extend the analysis to composite bodies such as dumbbells and Janus particles.

6.1. *Motion of two interacting particles*

Consider the motion of two spheres (labelled by 1 and 2) separated by a large distance R compared to their sizes a_1 and a_2. For particle i, its velocity $\boldsymbol{U}_i$ can be expressed as $\boldsymbol{U}_i = \boldsymbol{M}_i \cdot \boldsymbol{F}_i$ with $\boldsymbol{M}_i$ being the mobility tensor and $\boldsymbol{F}_i$ the net driving force on the particle. Here, the mobility tensor, because of the dumbbell-like geometry, is of the form $\boldsymbol{M}_i = M_{//}^{(i)} \boldsymbol{p}_i \boldsymbol{p}_i + M_{\perp}^{(i)}(\boldsymbol{I} - \boldsymbol{p}_i \boldsymbol{p}_i)$, where $M_{//}^{(i)}$ and $M_{\perp}^{(i)}$ denote the respective mobility coefficients along the centreline direction $\boldsymbol{p}_i$ ($= \boldsymbol{R}_i/R$ pointing away from the particle centre) and in the direction perpendicular to the centreline. Because the system configuration is axisymmetric with respect to the centreline, the reversibility of Stokes flow stipulates that the two particles will not rotate around, suggesting that they must be torque-free, i.e. $\boldsymbol{R}_i \times \boldsymbol{F}_i = 0$. Hence, the driving forces $\boldsymbol{F}_i$ will only be along the centreline and hence the particle velocities $\boldsymbol{U}_i$.

Suppose that either particle possesses a monopole-like potential $\Phi_i = (a_i/r_i)\tilde{\Phi}_i$, where $r_i = |\boldsymbol{x}_i|$ is the distance measured from the centre of particle i, and $\tilde{\Phi}_i$ is the corresponding potential scale with >0 (<0) denoting a source (sink). Clearly, each particle alone cannot be propelled by its own potential because of the isotropic potential energy distribution. As one particle can feel the potential field generated by its partner, a dipolar potential energy variation can be created around it and hence in turn produce a force to set it in motion. Therefore, the force on sphere i scales as the potential gradient generated by sphere j, giving

$$\boldsymbol{F}_i \sim -\nabla \Phi_j|_{x_j = R_j} = -\frac{\boldsymbol{p}_i}{R^2}\tilde{\Phi}_j a_j, \tag{6.1}$$

Note that this force can only act along the centreline because of torque free. Also, we use the fact that $\boldsymbol{p}_j = -\boldsymbol{p}_i$ to derive the result. Substitution (6.1) into the velocity–force relationship $\boldsymbol{U}_i = \boldsymbol{M}_i \cdot \boldsymbol{F}_i$ yields

$$\boldsymbol{U}_i \sim -M_{//}^{(i)} \boldsymbol{p}_i \frac{\tilde{\Phi}_j a_j}{R^2} \sim -\frac{\tilde{\Phi}_j}{\eta R^2}\boldsymbol{p}_i. \tag{6.2}$$

Here $M_{//}^{(i)} \sim 1/(\eta a_i)$ (its dependence on R can be negligible because of large R assumed here) and the contribution from the $M_{\perp}^{(i)}$ term vanishes because $M_{\perp}^{(i)}(\boldsymbol{I} - \boldsymbol{p}_i \boldsymbol{p}_i) \cdot \boldsymbol{F}_i = -M_{\perp}^{(i)}(\boldsymbol{I} - \boldsymbol{p}_i \boldsymbol{p}_i) \cdot \boldsymbol{p}_i \tilde{\Phi}_j a_j / R^2$ is identically zero. Equation (6.2) indicates that how one particle moves depends upon if its partner is a sink or source – it will be attracted towards (repelled by) its sink (source) partner with $\tilde{\Phi}_i < 0\,(>0)$. Similar to (4.5), (6.2) also implies the exactly same Coulomb-like feature: two sink (source) particles having $\tilde{\Phi}_i < 0\,(>0)$ will move towards (apart from) each other.

6.2. *Motion of dumbbells*

The above analysis can be extended to the motion of a dumbbell that comprises two spheres having a thin, rigid connector in between, as shown in figure 8. Since the net driving force $\boldsymbol{F} = \boldsymbol{F}_1 + \boldsymbol{F}_2$ generally does not vanish, the dumbbell must migrate along $\boldsymbol{F}$. Neglecting the drag of the connector, the velocity $\boldsymbol{U}$ of the dumbbell can be found by balancing $\boldsymbol{F}$ with the total drag force on the two spheres via $(\boldsymbol{M}_1^{-1} + \boldsymbol{M}_2^{-1}) \cdot \boldsymbol{U} = \boldsymbol{F}$, giving

$$\boldsymbol{U} \sim \frac{\boldsymbol{F}_1 + \boldsymbol{F}_2}{\eta(a_1 + a_2)} \sim \frac{(\tilde{\Phi}_1 a_1 - \tilde{\Phi}_2 a_2)}{\eta R^2 (a_1 + a_2)}\boldsymbol{p}_1. \tag{6.3}$$

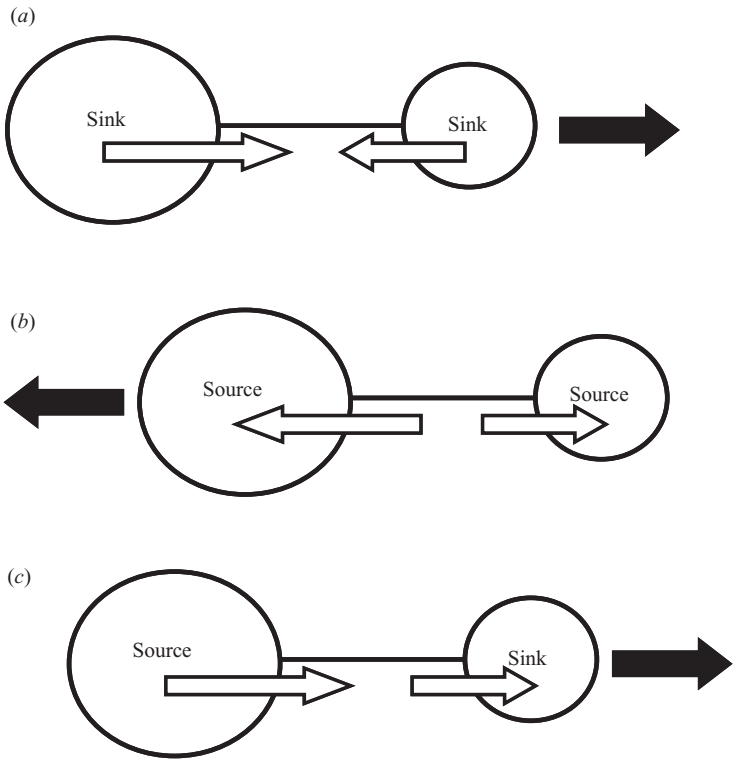

FIGURE 8. A schematic illustration of the self-motion of dumbbells. In (*a*), the dumbbell is made by two sink spheres which tend to move towards each other by inward forces. In (*b*), the dumbbell consists of two source spheres with outward forces that tend to pull them apart. In (*c*), the dumbbell constitutes a pair of sink and source spheres. For the sink (source) end, the exerted inter-particle force is pointed towards (away from) it. The inter-particle forces are indicated by white arrows. The motion directions of these dumbbells are indicated by black arrows.

Here we have used (6.1) together with $\boldsymbol{p}_2 = -\boldsymbol{p}_1$ to derive the result. Hence, the dumbbell will be powered by the weighted difference between $\tilde{\Phi}_1$ and $\tilde{\Phi}_2$, $(\tilde{\Phi}_1 a_1 - \tilde{\Phi}_2 a_2)/(a_1 + a_2)$. The direction of the dumbbell's motion is determined by the sphere having a larger force. If the dumbbell is made by two sink spheres (with $\tilde{\Phi}_1 < 0$ and $\tilde{\Phi}_2 < 0$), $\boldsymbol{F}^{(1)}$ and $\boldsymbol{F}^{(2)}$ will act inwards (see (6.1)). Thereby, the net force is towards the sphere having a smaller $|\tilde{\Phi} a|$ and so the direction of this sink-like dumbbell (figure 8*a*). Similarly, the motion of a source-like dumbbell (with $\tilde{\Phi}_1 > 0$ and $\tilde{\Phi}_2 > 0$) is led by the sphere with a larger $\tilde{\Phi} a$ (figure 8*b*). For a dumbbell made by an unlike pair, since both $\boldsymbol{F}^{(1)}$ and $\boldsymbol{F}^{(2)}$ act in the same direction from the source towards the sink, the motion is always led by the sink sphere (figure 8*c*).

6.3. *Motion of asymmetric shaped objects or Janus particles*

In this section, we further apply the above dumbbell analysis to explain the motion of an asymmetric shaped object or Janus-like particle (figure 9). In this case, we model a particle as a composite body of two spheres in contact or partially merged. In principle, one might have to include multipole contributions in the potential energy distribution to capture strong interactions between two touched spheres. As we have learned from the previous subsection that it is the dipolar contribution from the system orientation important to the motion, the use of the results using point-like

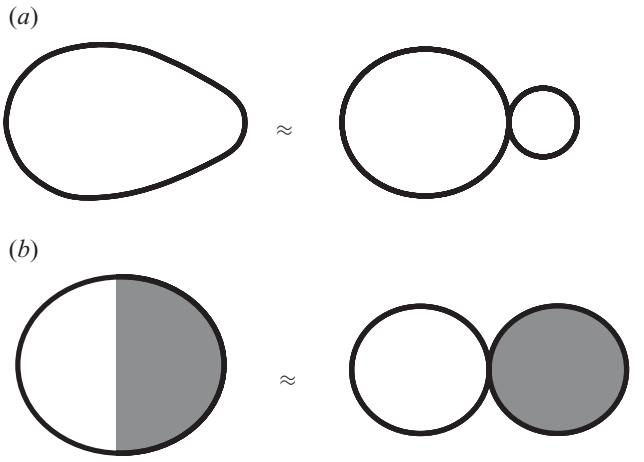

FIGURE 9. Approximate models for explaining the self-driven motion of an egg-shaped colloid (*a*) and that of a Janus particle (*b*). In (*a*), the colloid can be treated like a composite body made by two touched spheres of different sizes. In (*b*), the particle can be viewed as an object combining a pair of source and sink spheres in equal size.

approach in § 6.2 should, at least qualitatively, be able to reveal the features of the motion.

We first analyse the motion of a particle in asymmetric shape. For simplicity, we assume that this particle is egg-like. In this case, we can treat this particle as a composite body of two touched spheres in unequal sizes (figure 9*a*). Letting $\tilde{\Phi}_1 = \tilde{\Phi}_2 \equiv \tilde{\Phi}$ and $R = 2\bar{a} = a_1 + a_2$ in (6.3), we find that the velocity of the particle scales as

$$\boldsymbol{U} \sim \frac{\tilde{\Phi}(a_1 - a_2)}{\eta \bar{a}^3} \boldsymbol{p}_1. \tag{6.4}$$

As a result, if this egg-like particle is of sink (source) type with $\tilde{\Phi} < 0\,(>0)$, its motion will be towards the end with the smaller (larger) radius, as is shown in the dumbbell model. This result also provides a simpler explanation for the motion behaviour of a nearly spherical reactive particle shown in § 3.

A similar analysis can also be applied to the motion of a Janus-like particle which can be approximately treated as an object combining a pair of source and sink spheres in equal size (figure 9*b*). Letting $a_1 = a_2 = a$ and $R = 2\bar{a} = a_1 + a_2$ in (6.3), we find

$$\boldsymbol{U} \sim \frac{(\tilde{\Phi}_1 - \tilde{\Phi}_2)}{\eta a^2} \boldsymbol{p}_1. \tag{6.5}$$

Hence, the particle will migrate with the sink half being its front side.

7. Discussion

7.1. *Validity of the present analysis*

A few points concerning the validity of the present analysis are worth mentioning below. First of all, since we assume that the solute transport is governed by diffusion, our analysis holds if the convection induced by the particle drift is sufficiently weak compared to diffusion. That is, the Peclet number, the ratio of diffusion to convection

time scales, needs to be small,

$$Pe = \frac{Ua}{D} = \frac{\delta\alpha\, kTC_\infty a^2}{\eta D} \ll 1, \tag{7.1}$$

where the velocity scale $U = \delta\alpha kTC_\infty a/\eta$ with δ the small parameter (e.g. amplitude of surface undulation ε or $(a/R)^2$) measuring the degree of anisotropy. Assume that the dimensionless reactivity α is of an order of unity and $\delta \sim 10^{-1}$. With typical values $a \sim 1$ μm, $T \sim 300$ K, $\eta \sim 10^{-2}$ poise, and $D \sim 10^{-5}$ cm^{2}s^{-1}, our analysis is only applicable to systems containing a trace amount of reactive species at concentration C_∞ below 10^{-5} M. For $Pe \sim 10^{-1}$ or $C_\infty \sim 10^{-6}$ M, the particle drift will be an order of $U \sim 10$ μm s^{-1}. For larger solutes such as macromolecules or nanosized nuclei whose diffusion coefficients are much smaller (10^{-10} to 10^{-7}cm^2 s^{-1}), to attain a similar drift velocity, the required solute concentration will be of a few orders of magnitude higher, i.e. $C_\infty \sim 10^{-4}$ to 10^{-1} M.

However, if the particle drift is so fast that diffusion no longer dominates the transport, solutes will be advected by the fluid as the particle migrates. Because such advection can shrink the solute-depletion region on the particle's front and reduce the solute concentration in the trailing wake on the particle's rear (Squires & Brady 2005; Córdova-Figueroa & Brady 2008), the effect tends to reduce osmotic forces and thereby limits the speed of the particle. In fact, the particle velocity cannot grow indefinitely by raising the supply of reactants, since it never exceeds the diffusive velocity of reactants D/a (Córdova-Figueroa & Brady 2008).

Additionally, the transport of reactive solutes here is analysed on the 'quasi-steady' basis. This entails that the particle size does not change appreciably during its journey in which the particle is in fact shrinking or growing because of reaction. To see how fast the particle changes its size, we inspect solute balance over the particle: $4\pi a^2 \rho_s \mathrm{d}a/\mathrm{d}t = 4\pi a^2 D\, \boldsymbol{n}\cdot\nabla C|_{r=a} = 4\pi a^2 k_s C|_{r=a}$, where ρ_s is the density of solute molecule inside the particle. Substitution of (3.1) into the above equation yields the following equation governing how the particle size changes over time:

$$\left(1 + \frac{k_s a}{D}\right)\frac{\mathrm{d}a}{\mathrm{d}t} = \frac{k_s C_\infty}{\rho_s}. \tag{7.2}$$

Hence, the change in the particle size scales as $\Delta a \sim k_s t(1 + k_s a/D)^{-1} C_\infty/\rho_s$ which must be small compared to a for ensuring the present quasi-steady approach. Because the characteristic time scale is the particle translation time $t \sim L/U$ across the macroscopic length scale L (e.g. inter-particle distance or the size of the cell), a small change in the particle size during this period provides the condition under which the quasi-steady approach holds

$$\frac{\Delta a}{a} \sim \left(\frac{k_s}{a}\right)\left(\frac{L}{U}\right)\left(1 + \frac{k_s a}{D}\right)^{-1}\frac{C_\infty}{\rho_s} \ll 1. \tag{7.3}$$

In the diffusion limit $k_s a/D \gg 1$ (only for sink particles), $\Delta a/a \sim (D/a^2)(L/U)C_\infty/\rho_s$. In the reaction limit $k_s a/D \ll 1$, $\Delta a/a \sim (k_s/a)(L/U)C_\infty/\rho_s$. This approach, however, breaks down if the translation time L/U is too long compared to the diffusion time a^2/D (in the diffusion limit) or to the reaction time a/k_s (in the reaction limit). This is because the longer journey a particle experiences, the more apparent growth or shrinkage will result. In this case, a diffusive boundary layer grows like $(Dt)^{1/2}$ around the particle, which must be taken into account in the transient solute transport.

Nevertheless, the motion of reactive particles can still be thought at steady state in the low-Reynolds-numbers motion considered here, since any acceleration/deceleration of the particles will be dissipated by prevailing viscous effects and relaxed very quickly (within time $a^2\rho/\eta \sim 10^{-6}$ s for micrometre-sized particles in a fluid of density $\rho \sim 1$ g cm^{-3}).

7.2. *Screening length and collective flocculation in a suspension of sink particles*

In § 5.1, we have shown that a suspension of sink particles could undergo flocculation due to Coulomb-like attraction between these particles. If such flocculation indeed occurred, there could be clusters growing with time due to local accumulation of the particles. On the other hand, as the particles continue building up in clusters, particle concentration gradients are also developed between the clusters and the bulk solution, creating diffusion to oppose the clustering. Therefore, how strong this self-aggregation process depends upon the competition between the clustering and diffusion.

To quantify how strong the clustering is, we consider a suspension of sink particles of size a. Suppose that the clustering is initiated by a certain test particle, called 'nucleus', surrounded by a cloud of suspended particles of concentration ρ. Because of the reaction-induced attraction, there is an injection flux of the rate $\rho U \sim \rho\tilde{\Phi}/\eta r^2$ towards the nucleus, where the injection speed U (with $\tilde{\Phi} < 0$) can be estimated by (6.2) and r is the distance to the nucleus. At steady state, this convective flux is counterbalanced by the diffusive flux $-D_p\partial\rho/\partial r$ (with $D_p \sim kT/\eta a$ being the diffusivity of the particles), establishing the Poisson–Boltzmann distribution for $\rho(r \geqslant a)$:

$$\rho \sim \rho_0 \exp(\lambda/r), \tag{7.4}$$

where ρ_0 is the particle concentration in the bulk and λ represents the screening length

$$\lambda \sim \left|\tilde{\Phi}\right| / D_p\eta \sim \left|\tilde{\Phi}\right| a/kT. \tag{7.5}$$

As ρ is much larger than ρ_0 for $r < \lambda$ and decays very rapidly beyond λ, how strong the clustering is can be measured by the size of λ – the larger λ, the stronger the clustering. That is, λ is the characteristic length scale within which particle attraction is important. For $r > \lambda$, the particle distribution is not affected by the attraction and remains the same as that in the bulk. In other words, the attraction is 'screened'. This screening effect is attributed to zero net particle flux arising from the local Poisson–Boltzmann equilibrium established by a swarm of attracted particles around a nucleus – it tends to prevent further uptake of particles from the bulk towards the nucleus. The phenomenon is similar to the Debye screening on a charged object by its surrounding counterion cloud. During the clustering, the inward particle flux exceeds the outward diffusion flux until reaching the equilibrium at which particles cease to build up. As this injection process can only occur within λ but not outside λ, λ therefore measures the size of the zone within which particles can undergo collective attraction. The similar self-aggregation and screening length can also be found in thermocapillary nucleation of microdroplets (Karpov & Oxtoby 1997).

For a suspension of sink particles considered here, $\tilde{\Phi} \sim a^3kTC_\infty\gamma$ taken from the two-particle problem in § 4. Combining (7.5) with the diluteness condition $\gamma a^3 C_\infty \gg 1$ in (5.10), we find $\lambda \gg a$, suggesting that inter-particle attraction is virtually unscreened. Therefore, if the particle concentration $\rho_0 \sim \phi/a^3$ (with ϕ being the particle volume fraction) were so dense that the inter-particle distance $R_0 \sim \rho_0^{-1/3} \sim a/\phi^{1/3}$ becomes shorter than λ, the range of the clustering would become prohibitively long. This explains why a suspension of sink particles is susceptible to collective flocculation, as is discussed in § 5.1. The condition for flocculation $a/\phi^{1/3} < \lambda$ also agrees with (5.5).

7.3. *Comparison to pair propulsion by phoretic interactions*

In § 6, we have developed a scaling theory to explain the pairwise particle motion due to inter-particle interactions. It might be instructive to make a comparison with that due to phoretic interactions. In phoretic motion, since the screening length is typically much smaller than the particle size, potential variations are confined in the close vicinity of the particle surface. This effect results in an effective slip velocity of the surrounding fluid on the particle surface: $\boldsymbol{u}_s = b(\boldsymbol{I} - \boldsymbol{nn})\cdot\nabla\Phi$, with Φ being the driving potential and b the slip coefficient. It can be shown, with the aid of Lorentz reciprocal theorem (Happel & Brenner 1983), that a phoretic particle actually moves at the average slip velocity over the surface (Anderson 1985):

$$\boldsymbol{U}_{phoretic} = -bS_p^{-1}\int(\boldsymbol{I} - \boldsymbol{nn})\cdot\nabla\Phi\,\mathrm{d}A, \tag{7.6}$$

where S_p is the surface area of the particle. For spherical phoretic particles having uniform surface properties, similar to our two-particle problem they can also be self-driven by surface reactions (Golestanian *et al.* 2007) with potential variations created by particle interactions. In contrast to (6.2) for entropic swimmers, it is the 'surface gradient' of the potential, $(\boldsymbol{I} - \boldsymbol{nn})\cdot\nabla\Phi$, driving phoretic motion. To generate a non-zero $\boldsymbol{U}_{phoretic}$, $\nabla\Phi$ must be even in $\boldsymbol{n}$ and hence require at least a 'quadrupole' field $\nabla\Phi \sim (\boldsymbol{I} - 3\boldsymbol{xx}r^{-2})/r^3$ to set off the motion, as opposed to dipolar fields in entropic swimmers, where r is the inter-particle distance. Thereby, the phoretic velocity $\boldsymbol{U}_{phoretic}$ decays at the rate of r^{-3} faster than r^{-2} in entropic swimmers. In other words, the pair propulsion by entropic interactions is more efficient than that by phoretic interactions. In the latter, one would require more concentrated particles to render greater potential gradients for setting them in motion.

In analogy to thin and thick Debye layer limits in the context of electrophoresis, it can be thought that the present entropic swimming works in the 'unscreened' limit (see § 7.2), whereas phoretic swimming does in the 'screened' limit. Since the screening length measures the effective range of the propulsion force and is determined by the natures of solutes and particles, reactive particles in different solutions might display distinct motion and dispersion behaviours.

8. Concluding remarks

In conclusion, we have analysed the motion of reactive colloids and shown that they can be propelled by asymmetric osmotic forces generated by their own. The motion can occur due to asymmetry in the particle shape or to the presence of neighbouring particles. In the former, we find that a sink (source) particle can move with its sharp (blunt) end. In the latter, a pair of sink (source) particles can move towards (apart from) each other, resembling Coulomb-like attraction (repulsion). When two particles are nearly in touch, however, we show that the particle velocity will grow cubically with their separation. The opposite trends of the particle drift in small and large separation limits stipulate that the maximum thrust must exist at the crossover between these two limits in such a way that driving osmotic forces are enhanced by shortening the inter-particle distance while hydrodynamic drags are reduced by increasing the distance.

In light of the Coulomb-like nature of pair propulsion, we find that collective flocculation could likely occur to sink particles due to unscreened osmotic attraction (see § 5). Whether the flocculation can occur depends on three time scales: the collision time between two self-attracting particles, the diffusion time over the particle separation and the rotational diffusion time of the particles. Inspecting these time

scales, we can establish the criterion for an occurrence of the flocculation. Since Brownian randomization can be enhanced by reaction at high particle concentrations whereas osmotic forces become too sluggish to drive particles at low particle concentrations, we arrive at the conclusion that the flocculation can only occur in a certain range of the particle volume fraction, as is revealed by our scaling analysis.

The stability of reactive suspensions is also discussed in the modified DLVO framework and seems to be determined by the competition between long-range reaction-induced osmotic effects, short-range van der Waals attraction and Debye electrostatic repulsion.

We have also developed a scaling theory to elucidate the features of various self-driven motions such as two interacting particles, composite bodies and Janus particles. All are driven by dipolar distortions in potential energy. For the self-motion due to particle interactions, it admits R^{-2} decay in particle velocities and hence is more efficient than that due to phoretic interactions in which particles velocities vary as R^{-3}, where R is the inter-particle distance.

Our study might shed some light on other self-driven phenomena such as coarsening of microdrops (Tanaka 1996) and phase separation in nematic liquid crystals (Thakur *et al.* 2006). This is because in these phenomena coalescence of small nuclei and their growth into larger clusters are commonly involved and in essence resemble the flocculation of reactive colloids discussed in this work. It is also possible to incorporate our results into kinetic theories for describing evolution of microstructures in various processes such as heterogeneous nucleation, formation of nanocrystals, clustering in microemulsion and self-organization of anisotropic materials.

This work was supported by the National Science Council of Taiwan under Grant No. NSC 97-2628-E-006-001-MY3.

REFERENCES

Anderson, J. L. 1985 Effect of nonuniform zeta potential on particle movement in electric-fields. *J. Colloid Interface Sci.* **105**, 45–54.

Anderson, J. L. 1989 Colloid transport by interfacial forces. *Annu. Rev. Fluid Mech.* **21**, 61–99.

Ashkin, A., Dziedzic, J. M., Bjorkholm, J. E. & Chu, S. 1986 Observation of a single-beam gradient force optical trap for dielectric particles. *Opt. Lett.* **11**, 288–290.

Askura, S. & Oosawa, F. 1954 On interaction between two bodies immersed in a solution of macromolecules *J. Chem. Phys.* **22**, 1255–1256.

Batchelor, G. K. 1976 Brownian diffusion of particles with hydrodynamic interaction. *J. Fluid Mech.* **74**, 1–29.

Córdova-Figueroa, U. M. & Brady, J. F. 2008 Osmotic propulsion: the osmotic motor. *Phys. Rev. Lett.* **100**, 158303.

Córdova-Figueroa, U. M. & Brady, J. F. 2009 Comment on "Osmotic propulsion: the osmotic motor". Reply. *Phys. Rev. Lett.* **103**, 079802.

Córdova-Figueroa, U. M. & Brady, J. F. 2009 Comment on "Osmotic propulsion: the osmotic motor". Reply. *Phys. Rev. Lett.* **103**, 159802.

Crocker, J. C., Matteo, J. A., Dinsmore, A. D. & Yodh, A. G. 1999 Entropic attraction and repulsion in binary colloids probed with a line optical tweezer. *Phys. Rev. Lett.* **82**, 4352–4355.

Einstein, A. 1905 The motion of elements suspended in static liquids as claimed in the molecular kinetic theory of heat. *Ann. Phys.* **17**, 549–560.

Fischer, C. M. & Dhar, P. 2009 Comment on "Osmotic propulsion: the osmotic motor". *Phys. Rev. Lett.* **102**, 159801.

Golestanian, R., Liverpool, T. B. & Ajdari, A. 2005 Propulsion of a molecular machine by asymmetric distribution of reaction products. *Phys. Rev. Lett.* **94**, 220801.

Golestanian, R., Liverpool, T. B. & Ajdari, A. 2007 Designing phoretic micro- and nano-swimmers. *New J. Phys.* **9**, 126.

Happel, J. & Brenner, H. 1983 *Low Reynolds Number Hydrodynamics*. Prentice-Hall.

Hobson, E. W. 1965 *The Theory of Spherical and Ellipsoidal Harmonics*. Cambridge University Press.

Howse, J. R., Jones, R. A. L., Ryan, A. J., Gough, T., Vafabakhsh, R. & Golestanian, R. 2007 Self-motile colloidal particles: from directed propulsion to random walk. *Phys. Rev. Lett.* **99**, 048102.

Jones, T. B. 1995 *Electromechanics of Particles*. Cambridge University Press.

Jülicher, F. & Prost, J. 2009 Comment on "Osmotic propulsion: the osmotic motor". *Phys. Rev. Lett.* **103**, 079801.

Karpov, V. G. & Oxtoby, D. W. 1997 Self-organization of growing and decaying particles. *Phys. Rev.* E **55**, 7253–7259.

Morgan, H. & Green, N. G. 2003 *AC Electrokinetics*: *Colloids and Nanoparticles*. Research Studies Press.

Ogden, A. L. & Lewis, J. A. 1996 Effect of nonadsorbed polymer on the stability of weakly flocculated suspensions. *Langmuir* **12**, 3413–3424.

Paxton, W. F., Kistler, K. C., Olmeda, C. C., Sen, A., St. Angelo, S. K., Cao, T., Mallouk, T. E., Lammert, P. E. & Crepi, V. H. 2004 Catalytic nanomotors: autonomous movement of striped nanorods. *J. Am. Chem. Soc.* **126**, 13424–13431.

Pohl, H. A. 1978 *Dielectrophoresis*. Cambridge University Press.

Russel, W. B., Saville, D. A. & Schowalter, W. R. 1989 *Colloidal Dispersions*. Cambridge University Press.

Solomentstev, Y., Velegol, D. & Anderson, J. L. 1997 Conduction in the small gap between two spheres. *Phys. Fluids* **9**, 1209–1217.

Squires, T. M. & Brady, J. F. 2005 A simple paradigm for active and nonlinear microrheology. *Phys. Fluids* **17**, 073101.

Tanaka, H. 1996 Coarsening mechanisms of droplet spinodal decomposition in binary fluid mixtures. *J. Chem. Phys.* **105**, 10099–10114.

Thakur, S., Sunil Kumar, P. B., Madhusudana, N. V. & Pullarkat, P. A. 2006 Self-propulsion of nematic drops: novel phase separation dynamics in impurity-doped nematogens. *Phys. Rev. Lett.* **97**, 115701.

Tsao, H. K. 2001 Diffusion into a pair of reactive spheres with first-order reaction. *J. Chem. Phys.* **114**, 10247–10251.

Verwey, E. J. W. & Overbeek, J. Th. G. 1948 *Theory of the Stability of Lyophobic Colloid*. Elsevier.